Prepared for submission to JCAP

arXiv:1408.0233v2 [hep-ph] 6 Aug 2014

Nonabelian dark matter models for 3.5 keV X-rays

James M. Cline[a] **and Andrew R. Frey**[b]

[a]Department of Physics, McGill University, 3600 rue University, Montréal, Québec, Canada H3A 2T8

[b]Department of Physics and Winnipeg Institute for Theoretical Physics, University of Winnipeg, Winnipeg, Manitoba, Canada R3B 2E9

E-mail: jcline@physics.mcgill.ca, a.frey@uwinnipeg.ca

Abstract. A recent analysis of *XXM-Newton* data reveals the possible presence of an X-ray line at approximately 3.55 keV, which is not readily explained by known atomic transitions. Numerous models of eV-scale decaying dark matter have been proposed to explain this signal. Here we explore models of multicomponent nonabelian dark matter with typical mass $\sim$ 1-10 GeV (higher values being allowed in some models) and eV-scale splittings that arise naturally from the breaking of the nonabelian gauge symmetry. Kinetic mixing between the photon and the hidden sector gauge bosons can occur through a dimension-5 or 6 operator. Radiative decays of the excited states proceed through transition magnetic moments that appear at one loop. The decaying excited states can either be primordial or else produced by upscattering of the lighter dark matter states. These models are significantly constrained by direct dark matter searches or cosmic microwave background distortions, and are potentially testable in fixed target experiments that search for hidden photons. We note that the upscattering mechanism could be distinguished from decays in future observations if sources with different dark matter velocity dispersions seem to require different values of the scattering cross section to match the observed line strengths.

Keywords: dark matter theory

Contents

1 Introduction **1**

2 XDM and the observed signal **3**

3 General features of nonabelian DM models **5**

4 Doublet DM model **8**
4.1 Long-lived decaying DM 9
4.2 XDM doublet model 11

5 Triplet DM model **12**
5.1 Mass Splittings 13
5.2 Decaying DM Model 14
5.3 Triplet XDM 15

6 Discussion **17**

A Magnetic moments **18**

B CMB bounds from DM annihilation **20**

1 Introduction

Aside from its total mass density, little is known about the particle nature of dark matter (DM). Only upper limits exist on its possible nongravitational interactions with the Standard Model (SM), or on its self-interactions that could come from dynamics of a hypothetical dark sector extending beyond the dark matter itself. Hints of positive detection from a variety of direct searches [1–6] are in apparent conflict with limits from other experiments [7–11], presenting an increasingly difficult challenge for theorists to find nonminimal models that could accommodate both kinds of results. Anomalies in astrophysical observations have also been interpreted as harbingers of the interaction of dark matter with the visible sector. These include observations of excess positrons in the 10 GeV-TeV range [12–15], a narrow feature in gamma rays at 130 GeV [16, 17], a gamma ray excess at energies below 10 GeV [18–21], and the long-studied galactic bulge positron population [22, 23], among others, as candidate signals of DM. Whether any of these observations ultimately prove to be related to DM, they have led to a greater understanding of the range of physics possible in the dark sector.

Recently, refs. [24, 25] identified an X-ray line with energy of approximately 3.55 keV in *XMM-Newton* observations of galaxy clusters and the M31 galaxy, that is not associated with any known atomic transition that could be consistent with the observed intensity. The line also appears in *Chandra* observations of the Perseus cluster [24]. In the absence of a clear astrophysical explanation, the possibility that this line is associated with DM is tantalizing; as proposed by the original two references, the decay of a sterile neutrino to a photon and SM neutrino is a well-motivated DM explanation (see also [26–35]). Alternative light DM candidates suggested as the source of the X-ray line include axions and axion-like

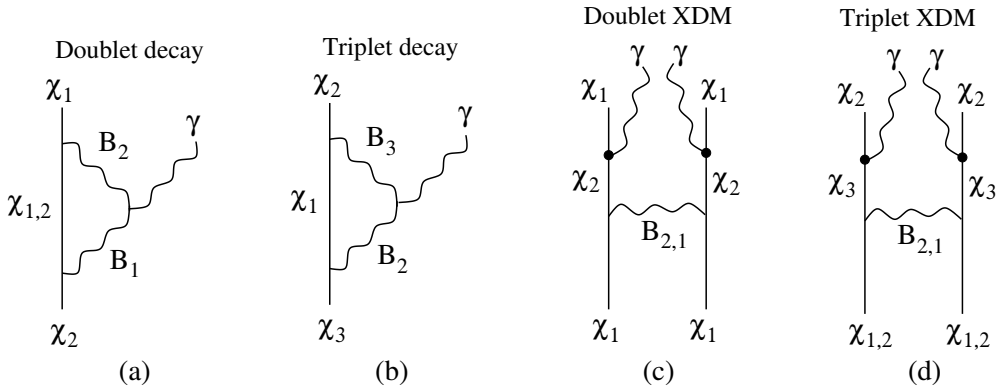

Figure 1. (a,b) Diagrams for slow decay of relic excited state to lower state in the doublet and triplet DM models, respectively; (c,d) upscattering of lighter DM states to excited state, followed by fast decays back to lower state (XDM mechanism), in respective models.

particles [36–40], axinos [41–43], moduli [44–46], light superpartners [47–50], and others [51–53]. It is also possible that more massive (GeV-scale or higher) multi-species DM with a transition dipole moment or other higher-dimension coupling can generate the 3.5-keV X-ray line [50, 54–60].

While recognizing that the slow decay of a relic excited DM state could account for the X-ray line, ref. [54] pointed out that collisional excitation of DM followed by a relatively rapid decay could also do so. This mechanism of exciting dark matter (XDM) leads to a distinct emission morphology (following the dark matter density profile squared rather than linearly) and was considered previously to address the galactic 511 keV emission (see [61–74]). In this paper, we will explore these scenarios in detail in the context of spontaneously broken nonabelian DM models, that can naturally have the necessary ingredients of small mass splittings [75] and kinetic mixing with the photon through a dimension-5 or 6 operator.

We consider relatively simple hidden sectors, in which the DM is a Dirac or Majorana fermion χ_a transforming as a doublet or triplet respectively of a hidden-sector SU(2) gauge symmetry. It is spontaneously broken by the vacuum expectation value (VEV) of a dark Higgs doublet in the doublet DM model, or by either two dark Higgs triplets or a doublet plus a triplet, in the triplet DM model. Significant kinetic mixing between the photon and one of the components of the dark gauge boson leads to a transition magnetic moment between DM states [68], by which the excited state can decay to a lower state and a photon, producing the 3.5 keV X-ray.[1] The excited state might either be primordial in origin, with relatively long lifetime to explain the observed line, or it could be produced by upscattering of the lower states, followed by fast decays. The relevant processes are depicted in fig. 1.

We begin in sect. 2 with a review of the observed X-ray line and the general requirements for decaying or XDM mechanisms to match the observed line strength. Section 3 describes generic theoretical predictions of the models that are relevant to our study, including kinetic mixing, relic density, mass splittings, magnetic moments, and cross sections for inelastic self-scattering as well as scattering on protons. In section 4 we confront these predictions

[1] Ref. [70] predicted, long before the 3.5 keV line, the existence of a several-keV X-ray line from exothermic models of XDM, but the expected value of flux was lower than required here, in the parameter space of interest for explaining excess low-energy galactic positrons.

to the experimental constraints on models of doublet dark matter, while section 5 does likewise for triplet DM. In section 6 we summarize our findings and discuss the relation of nonabelian DM models to other current anomalies that may be indirect signals of dark matter. Appendices give details of the computation of transition magnetic moments and cosmic microwave background (CMB) constraints.

2 XDM and the observed signal

We begin by summarizing the requirements on the lifetime or upscattering cross section from the observed line strength for the decaying or XDM mechanisms, respectively. For the decaying scenario, refs. [24, 25] found that the 3.5 keV line could be produced by sterile neutrino DM of mass $m_s \sim 7$ keV with a lifetime of $\tau_s \sim 6.2 \times 10^{27}$ s (ref. [25] gives errors of about a factor of 3 in either direction). Here we consider instead a heavy DM candidate with several nearly degenerate states, including a metastable one χ_x that decays to a lighter DM state plus a photon. Having in mind GeV-scale DM with a fractional abundance f_x in the excited state, the required lifetime is

$$\tau = f_x \left(\frac{m_s}{M_\chi}\right) \tau_s = (4.3 \times 10^{21}\,\mathrm{s})\, f_x \left(\frac{10\ \mathrm{GeV}}{M_\chi}\right) \implies \frac{\Gamma}{M_\chi} = \frac{1.5 \times 10^{-47}}{f_x}\ . \tag{2.1}$$

As in refs. [54–60], we are interested in a decay $\chi_x \to \chi_g \gamma$ to the ground state χ_g (or possibly to another long-lived excited state) plus a photon. In our models this occurs via a transition dipole moment $\mu_\times\, \bar{\chi}_x\, \sigma_{\mu\nu} \chi_g\, F^{\mu\nu}$. For mass splitting δM_χ, the decay rate corresponding to this operator is

$$\Gamma = \frac{4\mu_\times^2}{\pi}\, \delta M_\chi^3\ , \tag{2.2}$$

so the required dipole moment for the X-ray signal is

$$\mu_\times = \frac{1.7 \times 10^{-15}}{\mathrm{GeV}} \sqrt{\frac{M_\chi/f_x}{10\ \mathrm{GeV}}}\ . \tag{2.3}$$

On the other hand, if the transition dipole moment is larger than (2.3), the excited DM state will decay too rapidly, so there must be some mechanism to repopulate it. In XDM, this is accomplished through collisional excitation. In this case, the flux from a cluster or galaxy at distance d is

$$F = \frac{\eta_X f_g^2}{4\pi d^2 g_\chi} \int d^3x\, \frac{\rho_\chi^2}{M_\chi^2} \langle \sigma_\uparrow v_{\mathrm{rel}} \rangle \tag{2.4}$$

where $\sigma_\uparrow$ is the upscattering cross-section ρ_χ is the DM mass density; $f_g \sim 1$ is the fractional abundance of the DM ground state (or possibly a cosmologically long-lived excited state), $g_\chi = 2$ or 4 depending on whether the DM is Majorana or Dirac, and η_X is the number of X-rays produced per collision ($\eta_X = 2$ in our models). The cross section is dominated by contributions near the kinematic threshold, so we approximate

$$\begin{aligned} \langle \sigma_\uparrow v_{\mathrm{rel}} \rangle &= \sigma_0\, v_t\, \gamma; \\ \gamma &\equiv \left\langle \sqrt{v_{\mathrm{rel}}^2/v_t^2 - 1}\ \Theta(v_{\mathrm{rel}} - v_t) \right\rangle, \end{aligned} \tag{2.5}$$

where $v_t = \sqrt{8\,\delta m_\chi / M_\chi}$ is the threshold velocity for producing two excited states. For the phase space average, we assume a Maxwellian distribution $f(v) = N \exp(-(v/v_0)^2)$,

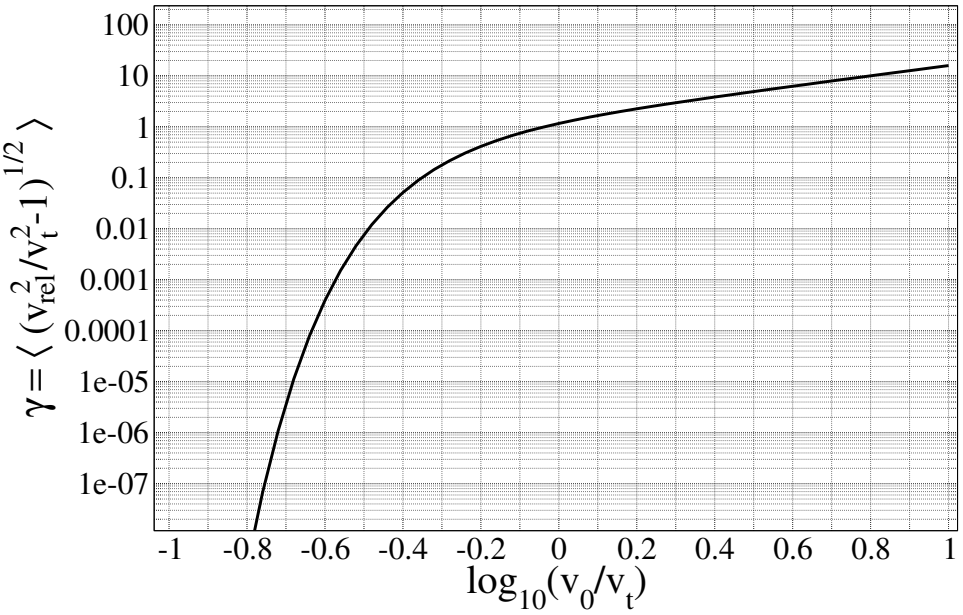

Figure 2. Phase space average of $(v_{\rm rel}^2/v_t^2 - 1)^{1/2}$, appearing in the upscattering cross section (2.5), for Maxwellian velocity distribution $\sim \exp(-(v/v_0)^2)$, as a function of v_0/v_t, where $v_t = \sqrt{8\delta M_\chi/M_\chi}$ is the threshold velocity.

where the velocity dispersion is $\sigma_v = \langle v^2 \rangle^{1/2} = \sqrt{3/2}\, v_0$. Refs. [76, 77] find $\sigma_v = 150$ km/s and 170 km/s respectively for M31; we take the median value 160 km/s $= 5.3 \times 10^{-4}\, c$. The corresponding value for the Perseus cluster is 1300 km/s [78, 79]. Fig. 2 shows the dependence of γ on v_0/v_t. If $v_0 \gg v_t$ for both M31 and the Perseus cluster, then the ratio of velocities $1300/160 = 8.1$ translates into a similar ratio of fluxes for the two systems. Below we will find a somewhat larger ratio $\gtrsim 20$. While the quality of the determinations is not sufficiently high to trust this number, if correct, it could be accommodated by taking $v_0 \cong 0.65\, v_t$ for M31, fixing $v_t \cong 6.7 \times 10^{-4}\, c$. With $v_0 \cong 0.3\, v_t$ in M31, we can explain a factor of 100 difference between the cross sections for the two systems.

To estimate the required cross section in (2.5), we compare to the observations of the X-ray flux for M31 and the Perseus cluster. The DM halo of M31 can be modeled by an Einasto profile

$$\rho(r) = \rho_{-2}\, \exp\left[-\frac{2}{\alpha}\left(\left(\frac{r}{r_{-2}}\right)^\alpha - 1\right)\right] \tag{2.6}$$

Ref. [80] finds two fits with $\alpha = 1/6$, normalization $\rho_{-2} = (8.9 \text{ or } 1.5) \times 10^{-2}$ GeV/cm^3, and scale radius $r_{-2} = (17.44 \text{ or } 37.95)$ kpc respectively. The field of view for the on-center observations of M31 reported in [25] is approximately 480 square arcmin, corresponding to a radius of 2.8 kpc at the distance $d = 785$ kpc, and the flux is $F \approx 5 \times 10^{-6}\, \text{s}^{-1}\text{cm}^{-2}$. Computing the volume integral in (2.4) using these two profiles, we estimate

$$\frac{\eta_X f_g^2 \langle \sigma v_{\rm rel} \rangle}{g_\chi M_\chi^2} \approx \left(5 \times 10^{-24} \text{ to } 3 \times 10^{-23}\right)\ \text{cm}^3\, \text{s}^{-1}\, \text{GeV}^{-2}\ . \tag{2.7}$$

(This is far below the limit $\langle \sigma v_{\rm rel} \rangle \lesssim 1$ b/GeV on the self-interactions of dark matter from observations of systems like the Bullet Cluster; see ref. [81] for a recent review.)

The analogous computation for the Perseus cluster gives a volume integral of

$$\frac{1}{4\pi d^2}\int d^3x\,\rho^2 \approx 10^{16.25}\ \mathrm{GeV}^2\,\mathrm{cm}^{-5} \tag{2.8}$$

for the entire cluster [82]. Ref. [83] finds the similar value $10^{16.15}$. The central value of flux from Perseus was measured to be $5.2\times10^{-5}\,\mathrm{cm}^{-2}\,\mathrm{s}^{-1}$ (MOS, [24]), $7.0\times10^{-6}\,\mathrm{cm}^{-2}\,\mathrm{s}^{-1}$ (MOS, [25]), or $9.2\times10^{-6}\,\mathrm{cm}^{-2}\,\mathrm{s}^{-1}$ (PN, [25]).[2] These yield

$$\frac{\eta_X f_g^2\,\langle\sigma v_{\rm rel}\rangle}{g_\chi M_\chi^2} \approx (5\times10^{-22}\ \text{to}\ 4\times10^{-21})\ \mathrm{cm}^3\,\mathrm{s}^{-1}\,\mathrm{GeV}^{-2}\ . \tag{2.9}$$

The cluster values are systematically higher than those of M31 by a factor of ~ 100. However the ranges in (2.7) and (2.9) are not necessarily correlated, so the actual ratio could smaller. In particular, if the true ratio is ~ 8, this would be consistent with $v_t \ll v_0$ in fig. 2, both for v_0 of M31 and of the Perseus cluster. In summary, the required cross sections are of order $f_g^2\,\langle\sigma_0\,v_{\rm rel}\rangle/M_\chi^2 \sim 10^{-22}\ \mathrm{cm}^3\,\mathrm{s}^{-1}\,\mathrm{GeV}^{-2}$ for M31, and $\sim 10-100$ times larger for Perseus, with the difference possibly being attributable to the higher DM velocities in the cluster.

3 General features of nonabelian DM models

Before investigating specific models with respect to the X-ray line, we summarize general features of the nonabelian DM models. We elaborate on results of ref. [68] concerning the kinetic mixing, mass splittings, magnetic moment, thermal relic density, self-scattering cross section, and interaction with nucleons here. The dark sector consists of a fermionic DM multiplet χ of mass M_χ transforming under a nonabelian gauge symmetry with vector bosons B_μ^a and coupling g. We will consider only the simplest case of SU(2) for our specific examples, but in this section we give some results for general SU(N). The symmetry is spontaneously broken by some combination of doublet/fundamental (h_i) or triplet/adjoint (Δ_a) dark Higgs fields, which leads to at least one component of B_a kinetically mixing with SM hypercharge through a dimension-5 or 6 operator,

$$\frac{1}{\Lambda}\Delta^a B_a^{\mu\nu}Y_{\mu\nu} \quad \text{or} \quad \frac{1}{\Lambda^2}(h^\dagger\tau^a h)\,B_a^{\mu\nu}Y_{\mu\nu} \tag{3.1}$$

where Λ is some heavy scale. Once the Higgs has gotten a VEV, this will lead to kinetic mixing of a particular component $\hat{a}$ of the vector with the photon, We normalize it in the conventional way as $-(\epsilon/2)B_{\mu\nu}^{\hat{a}}F_{\mu\nu}$. Diagonalizing the photon-$B^{\hat{a}}$ kinetic terms gives $B^{\hat{a}}$ a coupling of strength ϵe to the electromagnetic current, which is the main portal between the dark and visible sectors.

Relic density. We will be generally be interested in scenarios where the dark matter has a bare mass $M_\chi \gtrsim 1$ GeV, while the gauge bosons have masses m_{B_a} that are smaller. In the model where χ_i is a doublet of SU(2), this bare mass term only exists if χ is Dirac, whereas a triplet fermion can be Majorana. Therefore the doublet DM model has a global charge and can be asymmetric, whereas the triplet would be expected to get its relic density through thermal freeze-out. In such a case, assuming that Yukawa couplings of χ to the Higgs bosons are negligible, freeze-out is determined by $\chi\chi \to BB$ through the gauge interactions,

[2] MOS and PN refer to the two different types of CCD cameras on *XMM-Newton*, metal oxide semiconductor and pn-junction respectively.

and one can constrain the coupling strength $\alpha_g = g^2/4\pi$ via the relic density. Updating the results of ref. [70] in light of the more accurate relic density cross section of [84], we find

$$\alpha_g \approx 1.6 \times 10^{-4} \left(\frac{M_\chi}{10\ \text{GeV}}\right) \tag{3.2}$$

for the SU(2) triplet model, assuming $M_\chi \gtrsim 5$ GeV. According to ref. [68], the doublet model requires α_g to be 2.5 times larger,[3] assuming only the symmetric component contributes to the relic density, A larger gauge group or DM representation requires a smaller α_g. In the more general case where Yukawa couplings could be responsible for the relic density by annihilation into light Higgses, eq. (3.2) can be interpreted as an upper bound on α_g to avoid suppressing the relic density.

Mass splittings. Of particular importance to our discussion, the states of the DM multiplet are generically split in mass due to symmetry breaking, both via Yukawa couplings and by differing gauge boson masses entering the DM self-energies [75]. For $m_{B_a} \ll M_\chi$, the latter effect gives rise to a correction to the DM mass term,

$$M\delta_{ij} - \frac{\alpha_g}{2} \sum_{B_a} m_{B_a} \left(T^a T^a\right)_{ij} \tag{3.3}$$

For DM in the doublet representation of SU(2), the square of any generator (since it is a Pauli matrix) is the unit matrix, so no splitting arises from this mechanism, and we are forced to rely upon splittings generated by VEVs of dark Higgs fields that couple to χ. For other representations, if all gauge boson masses are the same, the correction is proportional to the quadratic Casimir times δ_{ij}, which leaves the states degenerate, but in general $\delta M_\chi \sim \alpha_g\, \delta m_B/2$, where δm_B is the typical splitting between the gauge boson masses. Assuming that $\delta m_B \sim m_{B_a}$ and α_g is given by (3.2) the desired δM_χ of 3.5 keV requires gauge boson masses of order 40 MeV$\times$(10 GeV$/M_\chi$). However it should be kept in mind that Yukawa couplings can allow for larger m_{B_a}, both by directly contributing to the mass splittings, and by allowing for smaller α_g as discussed above.

Magnetic moments. A unique feature of kinetic mixing in the form (3.1) is that it includes an interaction

$$\frac{1}{2} g \epsilon f^{\hat{a}bc} B^b_\mu B^c_\nu F^{\mu\nu} \tag{3.4}$$

by virtue of the nonabelian field strength tensor $B^{\hat{a}}_{\mu\nu}$. This operator generates transition (and in some cases direct) magnetic moments among the DM states, as shown in figure 1(a,b) [68]. We calculate the transition moments in appendix A. For models in which χ is in the triplet representation of SU(2), we can take $\hat{a} = 1$ and find that the transition moment between states 2 and 3 is given by[4]

$$\mu_{23} = \frac{\epsilon g^3}{16\pi^2\, M_\chi} F_t(r_2, r_3) \tag{3.5}$$

where $r_i = (m_{B_i}/M_\chi)^2$. The function F_t is given in (A.6), but can be approximated as

$$F_t \sim \ln\left(\frac{M_\chi}{\bar{m}}\right) - 1 \tag{3.6}$$

[3] Ref. [70] did a more careful computation of the triplet model relic density than [68], so we take the value of α_g from the former reference, rescaled by the group theory factors found in the latter for the case of the doublet model.

[4] We have corrected several factors of 2 relative to [68].

if $\bar{m}^2 \equiv (m_{B_2}^2 + m_{B_3}^2)/2 \ll M_\chi^2$ and if $|m_{B_2} - m_{B_3}|$ is not too large compared to m_{B_1}. The behavior of F_t is more generally illustrated in fig. 3, which shows that (3.6) is valid for $\bar{m} \lesssim M_\chi/10$; above that value, $\mu_\times$ is of order $\mathcal{O}(0.1-1)\epsilon g^3/16\pi^2 M$. For models in which χ is an adjoint of SU(N), eq. (3.5) is generalized by including the factor $(i/2)C_2(A)T^{\hat{a}}_{23}$ where $C_2(A)$ is the quadratic Casimir of the adjoint representation.

In models of doublet DM with kinetic mixing of B_3, fig. 1(a), there is destructive interference between the two diagrams where χ_1 and χ_2 are in the loop, leading to a suppressed transition moment

$$\mu_{12} = \frac{\epsilon g^3\, \delta M_\chi}{16\pi^2\, M_\chi^2} F_d(r) \tag{3.7}$$

where we ignore the gauge boson mass splittings (which anyway vanish if SU(2) is broken only by a Higgs doublet) and take $r = (m_B/M_\chi)^2$. The function F_d is given in (A.11) and behaves as $1/2r$ for small r, showing that the suppression is less severe than at first sight: $\mu_{12} \sim \delta M_\chi/m_B^2$ rather than $\delta M_\chi/M_\chi^2$.

Inelastic self-scattering. The excitation of lower to higher DM states by inelastic scattering, as shown in fig. 1(d) for the triplet model, has the cross section

$$\langle \sigma_\uparrow v_{\rm rel} \rangle = 2\pi\alpha_g^2\, v_t\, \gamma\, \frac{M_\chi^2}{m_B^4} \mathcal{F}(v_{\rm rel}/v_t) \tag{3.8}$$

where γ is as defined in (2.5) and $\mathcal{F}$ is a slowly varying function that goes to unity near threshold [70]. (Recall that $v_t = (8\,\delta M_\chi/M_\chi)^{1/2}$ is the threshold velocity for the inelastic process.)

In the doublet model, two components of the gauge bosons are exchanged in the t, u-channels. There is a cancellation in the $\chi_1\chi_1 \to \chi_2\chi_2$ amplitude that is exact in the case of degenerate gauge bosons, due to the group theory factors $\sum_{a=1,2}(\tau^a_{12})^2 = 0$. This changes the cross section by the replacement

$$m_B^{-4} \to (m_{B_1}^{-2} - m_{B_2}^{-2})^2 \equiv \frac{(\delta m_B^2)^2}{m_B^8} \tag{3.9}$$

relative to (3.8). In the following, we will assume that the XDM doublet is asymmetric dark matter with such a gauge boson mass splitting, which requires the VEV of a triplet Higgs in the dark sector, in addition to the doublet Higgs, since $\delta m_B = 0$ with only the latter.

Interaction with protons. Due to the kinetic mixing of $B^{\hat{a}}$ with the photon, the component $B^{\hat{a}}$ couples with strength ϵe to protons, and thus mediates DM interactions with nuclei. (There is a similar but much smaller contribution from the Z boson that we ignore.) The spin-independent cross section on protons is

$$\sigma_p = 16\pi\epsilon^2\, \alpha\, \alpha_g\, \frac{\mu_p^2}{m_B^4} \tag{3.10}$$

where μ_p is the proton-χ reduced mass. This will give rise to stringent constraints from direct detection searches for some of the scenarios we study in the remainder.

While the doublet DM model presented in section 4 scatters elastically from nuclei, the Majorana triplet DM models of section 5 scatter inelastically (either endothermically or exothermically). Since our focus is on astrophysical signals, we do not carry out a detailed analysis of the effects of this inelasticity on the nuclear recoil spectrum but rather consider

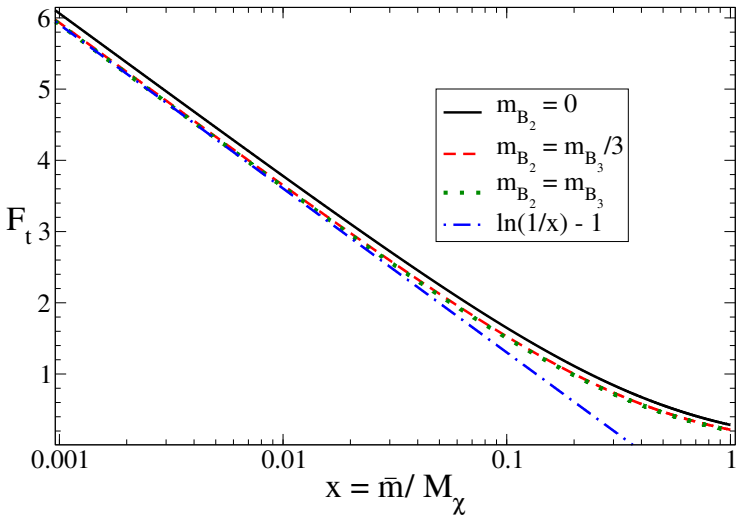

Figure 3. The transition magnetic moment for triplet DM generated by kinetic mixing of a non-Abelian gauge group with the photon, $F_t(r_2, r_3)$ of (3.5). $\bar{m}^2 = (m_{B_2}^2 + m_{B_3}^2)/2$, and the relation of m_2 to m_{B_3} is labeled as in the legend for each curve. The (blue) dot-dashed curve is the $\bar{m} \ll M_\chi$ approximation (3.6).

only the kinematic scaling of the overall event rate as in [70]. For endothermic or exothermic scattering, we rescale σ_p by

$$\left\langle (v^2 \mp v_\delta^2)^{1/2}\, \Theta(v \mp v_\delta) \right\rangle / \langle v \rangle, \qquad v_\delta = \left(\frac{2|\delta M_\chi|}{\mu_{N\chi}} \right)^{1/2} \tag{3.11}$$

respectively, where $\langle \cdots \rangle$ denotes the phase-space average in the standard halo model as described in [85], v is the DM speed in the earth frame, v_δ is the threshold velocity for nuclear scattering, and $\mu_{N\chi}$ is the reduced mass for the χ-nucleus system. We will find that LUX is the most constraining experiment for the inelastic models, and will therefore take xenon as the relevant nucleus for determining $\mu_{N\chi}$.

4 Doublet DM model

In the simplest version of doublet DM, χ is a Dirac field that has bare mass term $M_\chi \bar{\chi}^i \chi_i$. However, as noted above, the radiative correction to the mass of the doublet states is proportional to the identity matrix and leads to no mass splitting. There are two ways to remedy this situation. (1) Introduce a heavy SU(2)-singlet fermion ψ with mass M_0 (that we take to be Dirac) and with couplings $y\bar{\chi}h\psi$ + h.c.. If h gets the VEV $(v, 0)^T$ in just the upper component (as we can choose with no loss of generality), then χ_1 and χ_2 get a mass splitting by the see-saw mechanism of $\delta M_\chi = (yv)^2/M_0$. (2) Enlarge the dark gauge group to SU(2)×U(1) and break it to U(1) by the Higgs doublet, just as in the standard model. This splits the gauge boson masses analogously to the W and Z. Moreover, simple kinetic mixing of the dark U(1) with the SM hypercharge would lead to the same structure of couplings as we outlined previously. In addition, the dark W bosons would be millicharged under electromagnetism. Although option (2) may be interesting, we will confine our attention to the first in this work, which is simpler in having no extra long-range forces to consider.

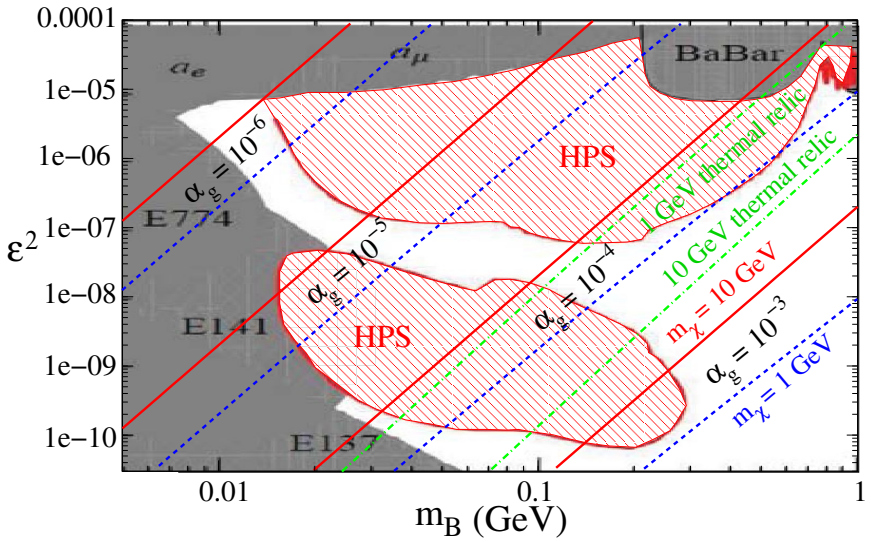

Figure 4. Dark shaded regions are excluded by searches for light gauge bosons of mass m_B coupling with strength ϵe to electrons; cross hatched region is to be probed by HPS experiment. Diagonal lines are the values of ϵ needed for doublet DM model to explain the 3.5. keV X-ray line via decays of a long-lived excited state, assuming indicated values of gauge coupling α_g and mass M_χ. Dot-dashed lines assume value of α_g needed for thermal relic density of χ. Background taken from ref. [86].

4.1 Long-lived decaying DM

We start with the scenario where χ_2 is cosmologically long-lived and decays into $\chi_1 + \gamma$. By combining eq. (2.3) with (3.7), we find the constraint on the kinetic mixing parameter

$$\epsilon = \frac{1.5 \times 10^{-10}}{\alpha_g^{3/2}\,\hat{F}_d(r)} \left(\frac{0.5}{f_x}\right)^{1/2} \left(\frac{M_\chi}{10\text{ GeV}}\right)^{1/2} \left(\frac{m_B}{100\text{ MeV}}\right)^2 \tag{4.1}$$

where $r = (m_B/M_\chi)^2$ and $\hat{F}_d = 2rF_d$ such that $\hat{F}_d$ goes from 1 to ~ 1.5 for $r \in [0,1]$, and is approximated to better than 1% by $\hat{F}_d \cong 1 + 0.716\,r^{1/2} - 0.248\,r$ in that interval.

It is interesting to compare the prediction of (4.1) to the sensitivity of existing and proposed searches for dark photons. In fig. 4 we show the targeted region of the HPS (Heavy Photon Search) experiment [86] in the m_B-ϵ plane, and the constraint (4.1), assuming different values for α_g and M_χ, and the relative abundance $f_x = 0.5$ for the excited state. Regions of constant α_g are bounded by the solid and dashed lines, corresponding to $M_\chi = 10$ and 1 GeV, respectively. We note that there is intersection with the cross-hatched HPS regions of interest for a wide range of gauge couplings. Although the doublet model can be asymmetric and thus free from the constraints associated with a thermal origin, we also show as dot-dashed lines the contours of $\alpha_g = 4 \times 10^{-4}(M_\chi/10\text{ GeV})$ as needed for the thermal relic density, for $M_\chi = 10$ and 1 GeV. These also have significant overlap with the HPS regions, making this model more testable than many others that have been proposed to explain the 3.5 keV X-ray line. Gauge couplings lower than the relic density bound need not be excluded even for asymmetric DM, since there is another possible annihilation channel

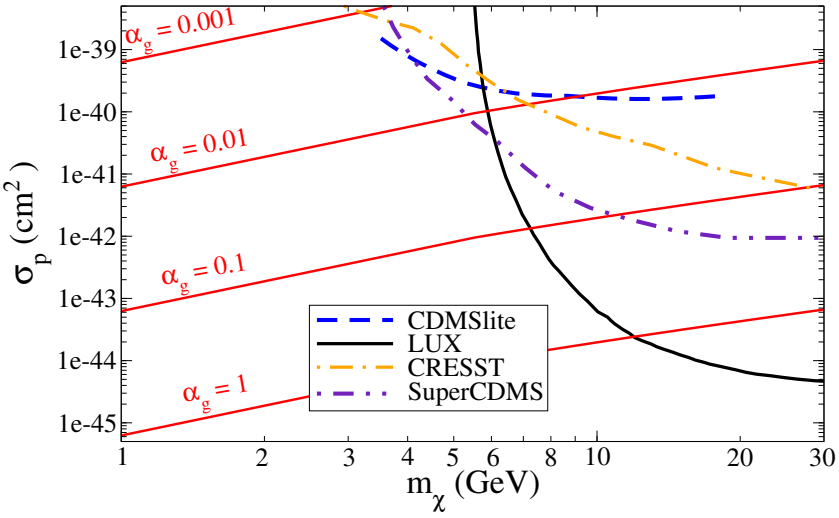

Figure 5. Cross section for doublet DM scattering on protons versus M_χ, in the slowly decaying DM scenario, along with current experimental limits. Diagonal lines correspond to the model predictions for the indicated values of gauge coupling, $\alpha_g = 10^{-3}, \ldots, 1$, assuming ϵ is given by (4.1).

$\chi\chi \to hh$ through the Yukawa interaction that splits the χ masses. This channel could be responsible for depleting the symmetric component of χ for small values of α_g.

We can also compare (4.1) to constraints from direct detection searches, since the cross section for χ scattering on protons goes as ϵ^2, eq. (3.10). Interestingly, for $m_B \ll M_\chi$, the m_B-dependence cancels between (4.1) and (3.10) allowing for predictions of $\sigma_p(M_\chi)$ that depend upon only one unknown parameter, α_g. Eliminating ϵ leads to the cross section on protons

$$\sigma_p = \frac{4 \times 10^{-45}\,\mathrm{cm}^2}{\alpha_g^2} \left(\frac{0.5}{f_x}\right) \left(1 + \frac{m_p}{M_\chi}\right)^{-2} \left(\frac{M_\chi}{10\ \mathrm{GeV}}\right) \tag{4.2}$$

In fig. 5 we show the predicted value of σ_p versus M_χ for a range of fixed α_g, along with the current upper limits from the LUX [10], CDMSlite [11], SuperCDMS [87], and CRESST [88] experiments. We have relaxed the published limits of the experiments by the factor $(Z/A)^2$ appropriate for each one, to account for our model coupling only to protons and not all nucleons. (For CRESST, it is assumed that the tungsten component gives the dominant constraint.) It is clear that mainly models with large values of $\alpha_g \gtrsim 10^{-3}$ that would pertain to asymmetric DM are constrained by direct detection, and that M_χ must be rather small, $\lesssim 10$ GeV, to escape detection. Comparison with fig. 4 shows the complementarity of direct detection and electron beam dump experiments for constraining the model. Only in the case $\alpha_g \sim 10^{-3}$, $M_\chi \sim 3$ GeV could there be some overlap in coverage, allowing for discovery by both kinds of experiments.

In terms of indirect limits, the strongest constraint on decaying DM comes from distortions of the cosmic microwave background due to injection of electromagnetic energy at the time of recombination [89–95]. Usually this is presented as a lower limit on the lifetime τ as a function of mass M_χ, assuming that all the mass-energy goes into ionizing radiation. If only a fraction $\delta M_\chi/M_\chi$ does so, the constraint on the lifetime is loosened by this factor. There can be a compensating factor of $\mathcal{O}(1)$ for the greater efficiency of absorption of keV

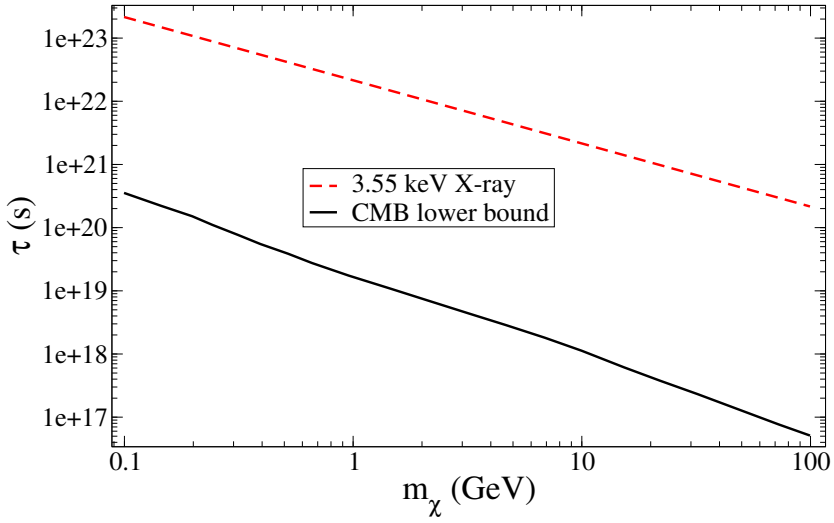

Figure 6. Solid curve: CMB lower bound on lifetime of excited state versus mass for decays into 3.55 keV X-ray, adapted from ref. [95]. Dashed: required value from 3.55 keV line strength, eq. (2.1).

energies relative to multi-GeV's [93], but this does not affect our conclusions. We replot the strongest constraint from ref. [95] in fig. 6 taking account of this factor. We have also applied an additional correction factor of 3.55 (no relation to the energy of the X-ray line) for the relative ionization efficiencies of photons and electrons [94] that further weakens their limit. The result is several orders of magnitude weaker than what is required to get the observed 3.55 keV line strength, eq. (2.1), also plotted in the figure.

4.2 XDM doublet model

As explained in section 3, it is necessary to introduce a mass splitting between the $B_{1,2}$ gauge bosons in order to have nonvanishing inelastic scattering $\chi_1\chi_1 \to \chi_2\chi_2$ for asymmetric doublet DM.[5] For example a triplet Higgs with VEV $\langle\Delta^a\rangle = \Delta\delta_{a,1}$ splits the gauge boson masses by $m_{B_2}^2 - m_{B_1}^2 = m_{B_3}^2 - m_{B_1}^2 = g^2\Delta^2$ [68].

In the scenario where $\chi_1\chi_1 \to \chi_2\chi_2$ produces the excited state, we can constrain m_B by equating the theoretical upscattering cross section (3.8, 3.9) to one of the observational estimates in (2.7) or (2.9). For definiteness, taking the lower value of (2.9) we find

$$m_B \cong \left(\frac{\delta m_B}{m_B}\right)^{1/2} \left(\frac{\alpha_g^{1/2}}{0.1}\right) \frac{(v_t\gamma)^{1/4}}{0.1} \times 280 \text{ MeV} \tag{4.3}$$

where γ is the quantity plotted in fig. 2.

A further requirement in this scenario is that the excited state must decay faster than the current Hubble rate. But in that case, CMB constraints are important, and in fact require that the lifetime be less than approximately 10^{12} s, so that primordial contributions have disappeared before the era of recombination (see for example ref. [93]). This puts a

[5] One might also consider symmetric doublet DM, in which the inelastic scattering $\chi_1\bar{\chi}_1 \to \chi_2\bar{\chi}_2$ can proceed through the s channel. But it turns out that this gives too small a cross section to explain the X-ray signal if α_g is as small as required by the thermal relic density constraint (3.2).

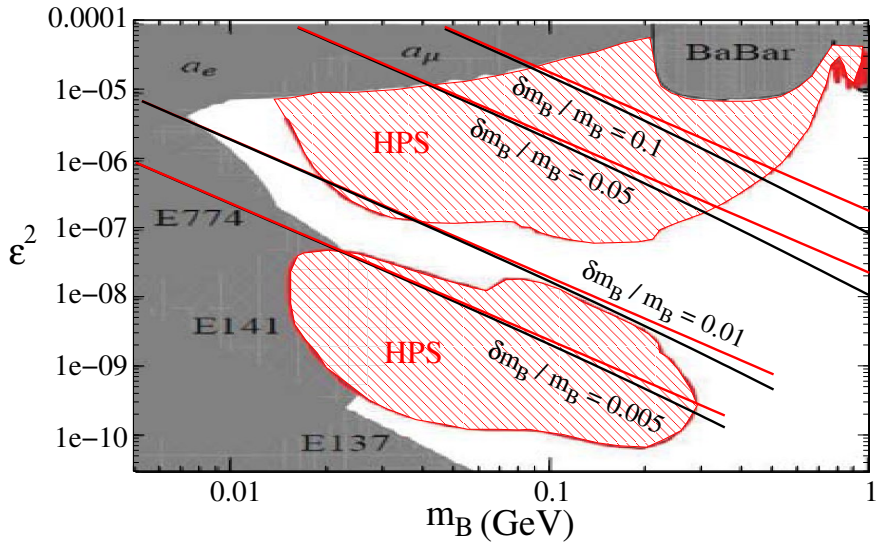

Figure 7. Like fig. 4, but for the XDM version of the doublet model. Here the diagonal lines are *lower bounds* from the requirement of sufficiently fast decay of the excited state. α_g varies from 10^{-4} to 1 as m_B increases. Upper (red) curves correspond to $M_\chi \gtrsim 10$ GeV, while lower (black) are for $M_\chi = 1$ GeV. Gauge boson mass splitting varies from $\delta m_B/m_B = 0.005$ to 0.1 as indicated.

lower bound on the kinetic mixing:

$$\epsilon > \frac{1.1\times 10^{-6}}{\alpha_g^{3/2}\hat{F}_d(r)}\left(\frac{m_B}{100\,\mathrm{MeV}}\right)^2 = \frac{0.09}{\hat{F}_d(r)}\left(\frac{\delta m_B}{m_B}\right)\left(\frac{v_t\gamma}{\alpha_g}\right)^{1/2} \tag{4.4}$$

where we used (4.3) to get the second expression. To compare with the sensitivity region of the HPS experiment, we vary α_g between 10^{-4} and 1 to generate parametric curves of ϵ versus m_B from (4.3) and (4.4), assuming $v_t\gamma = 10^{-3}$ for definiteness, and considering $\delta m_B/m_B$ and M_χ for several discrete values. The result is shown in fig. 7. Since these curves only indicate lower bounds on ϵ, there is considerable overlap between these predictions and the reach of HPS.

Moreover, (4.4) gives a lower bound for the cross section on protons from (3.10),

$$\sigma_p > \frac{10^{-36}\,\mathrm{cm}^2}{\alpha_g^2\,\hat{F}_d^2}\left(1+\frac{m_p}{M_\chi}\right)^{-2} \tag{4.5}$$

This constrains $M_\chi <$ a few GeV in order to evade direct detection. (Such small masses could be dangerous from the point of view of CMB constraints on annihilations resulting in electrons, except that we have assumed the doublet is asymmetric dark matter in the XDM scenario.) The XDM version of the model thus predicts an enormous signal for future low-threshold direct detection experiments that would be sensitive to light dark matter.

5 Triplet DM model

Unlike doublet representation DM, in which both components couple equally to all gauge bosons, triplet DM components χ_a each couple only to two of the three SU(2) gauge bosons

B^a. As a result, radiative corrections lead to mass splittings of order $\delta M_\chi \sim \alpha_g\, \delta m_B/2$ as in (3.3). Gauge boson mass differences of $\delta m_B \sim 45$ MeV$\times$(10 GeV$/M_\chi$) therefore lead to the appropriate splitting of $\delta M_\chi = 3.55$ keV. We will take χ_a to be Majorana for simplicity.

5.1 Mass Splittings

We consider two different dark Higgs sectors that turn out to have interestingly different predictions for direct detection, due to the spectra of gauge boson masses. In the first case, there are two triplet Higgs fields, denoted Δ^a and Δ'^a, with VEVs $\Delta^1 = \Delta\delta^{a1}$ and $\Delta'^a = \Delta'\delta^{a2}$. For simplicity we take only one of Δ, Δ' to appear in the kinetic mixing operator (3.1), so that only one gauge boson mixes with the photon.[6] In the second case, there is a single triplet Higgs Δ^a with VEV $\Delta^a = \Delta\delta^{a2}$ and a doublet Higgs h with VEV $(v/\sqrt{2})(1,1)^T$. Again for simplicity we assume that only one of these fields appears in the kinetic mixing (3.1).[7]

In either case, symmetries forbid any Yukawa couplings, so the DM mass splittings come exclusively from radiative corrections and for triplet DM take the form $\delta M_{ab} \equiv M_{\chi_b} - M_{\chi_a} = \alpha_g(m_{B_b} - m_{B_a})/2$. With two triplet Higgs fields, the gauge boson masses are

$$m_{B_1} = g\Delta', \quad m_{B_2} = g\Delta, \quad m_{B_3} = g\sqrt{\Delta^2 + \Delta'^2}, \tag{5.1}$$

giving rise to radiative DM mass splittings [68]

$$\delta M_{12} = \frac{1}{2} g\alpha_g \left(\Delta - \Delta'\right), \qquad \delta M_{23} = \frac{1}{2} g\alpha_g \left(\sqrt{\Delta^2 + \Delta'^2} - \Delta\right), \tag{5.2}$$

where χ_3 is the heaviest DM state and has a transition magnetic moment with either χ_1 or χ_2. With doublet and triplet Higgs (whose VEV is in the 2-direction), the gauge boson masses are

$$m_{B_1} = m_{B_3} = g\sqrt{v^2 + \Delta^2}, \quad m_{B_2} = gv \tag{5.3}$$

corresponding to DM mass splittings

$$\delta M_{21} = \delta M_{23} = \frac{1}{2} g\alpha_g \left(\sqrt{v^2 + \Delta^2} - v\right). \tag{5.4}$$

χ_2 is the lightest state, and χ_1, χ_3 are degenerate. We have chosen the h VEV $= (v, v)^T/\sqrt{2}$ so that kinetic mixing of B_1 generates a transition magnetic moment between χ_3 and χ_2.

If all the Higgs VEVs are of the same order of magnitude and the DM is produced thermally (so that α_g is determined by (3.2)), then $\{\Delta, \Delta', v\} \sim 1$ GeV $\times$ (10 GeV$/M_\chi)^{3/2}$ and therefore gauge boson masses of order 45 MeV$\times$(10 GeV$/M_\chi$) yield the desired 3.55 keV mass splitting. On the other hand, we can obtain δM_{23} =3.55 keV if $\Delta \gg \Delta'$ or $v \gg \Delta$ for the two Higgs sectors respectively, leading to mass splittings

$$\delta M_{23} = \frac{1}{4} g\alpha_g \left\{\frac{(\Delta')^2}{\Delta}, \frac{\Delta^2}{v}\right\}, \tag{5.5}$$

This gives $(\Delta')^2 = \Delta \times$ (2 GeV)(10 GeV$/M_\chi$) in the case of two triplets, and gauge boson masses $m_{B_1} \gtrsim 400$ MeV and $m_{B_{2,3}} \gtrsim 2$ GeV, with approximate equality at $\Delta \sim 5\Delta'$. With one doublet and one triplet Higgs, all the gauge boson masses are $m_{B_a} \gtrsim 2$ GeV. Nonthermal production of DM requires a larger gauge coupling and therefore allows for smaller Higgs VEVs and gauge boson masses.

[6] More generally, if the VEVs are not quite orthogonal, the other gauge bosons pick up (smaller) kinetic mixings, as well, without changing the conclusions below in a substantial way.

[7] Throughout, we take $\Delta, \Delta', v > 0$ without loss of generality.

5.2 Decaying DM Model

For triplet DM, the transition dipole moment $\mu_\times$ is given by (3.5). If the X-ray line is produced through long-lived excited state DM decay, the kinetic mixing parameter is

$$\epsilon = \frac{1.1\times10^{-13}}{\alpha_g^{3/2}F_t(r_2,r_3)}\left(\frac{0.3}{f_3}\right)^{1/2}\left(\frac{M_\chi}{10\text{ GeV}}\right)^{3/2}, \tag{5.6}$$

where $r_{2,3} = (m_{B_{2,3}}/M_\chi)^2$. Recall that the B_1 gauge boson is the one that mixes with the photon, and its mass depends on the dark Higgs sector of the model. In models with symmetry broken either by two triplet Higgs fields or by a triplet and a doublet, eqs. (5.1-5.4) imply that $m_{B_3} - m_{B_2} = 45\text{ MeV}\times(10\text{ GeV}/M_\chi) \equiv f(M_\chi)$; however $m_{B_1} = m_{B_3}$ for doublet plus triplet Higgses whereas $m_{B_1}^2 = m_{B_3}^2 - m_{B_2}^2$ for two triplets. This leads to the gauge boson mass relations

$$\begin{aligned} m_{B_2} &= m_{B_1} - f, & m_{B_3} &= m_{B_1}, & &\text{doublet + triplet Higgses} \\ m_{B_2} &= \frac{1}{2}(m_{B_1}^2/f - f), & m_{B_3} &= \frac{1}{2}(m_{B_1}^2/f + f), & &\text{two triplet Higgses} \end{aligned} \tag{5.7}$$

which fixes $m_{B_{2,3}}$ in terms of m_{B_1} and M_χ in what follows.

With any of the mass splittings and gauge boson masses discussed in section 5.1, the fractional relic abundance of χ_3 is $0.1 \lesssim f_3 \lesssim 0.33$ for thermal relic DM, as we have verified using the methods described in [70]. Since F_t runs between approximately 1/2 and 4 in the parameter space of interest, we find a required kinetic mixing $\epsilon \lesssim 10^{-8}$, which avoids current laboratory constraints on light vector bosons (summarized in [96]). However constraints on supernova cooling require $m_{B_1} \gtrsim 100$ MeV for $10^{-10} \lesssim \epsilon \lesssim 10^{-7}$ [97]. Nonthermal DM production necessitates a stronger gauge coupling, which further suppresses the required kinetic mixing.

Using (5.6) and (3.2) (assuming thermal production of the DM), we can eliminate ϵ and α_g from the predicted cross section (3.10) for scattering on protons,

$$\sigma_p = \frac{5.9\times10^{-43}\text{ cm}^2}{F_t(r_2,r_3)^2}\left(\frac{0.3}{f_3}\right)\left(1+\frac{m_p}{M_\chi}\right)^{-2}\left(\frac{M_\chi}{10\text{ GeV}}\right)\left(\frac{100\text{ MeV}}{m_{B_1}}\right)^4, \tag{5.8}$$

recalling that the gauge boson masses are related as in (5.7), depending on the choice of Higgs sector. Scattering from nuclei in direct detection experiments can either be endothermic $\chi_2 N \to \chi_3 N$ or exothermic $\chi_3 N \to \chi_2 N$ events, since both states are populated at present day. The state χ_1 does not participate in nuclear scattering.

However, limits on σ_p from direct detection experiments are expressed in terms of cross sections for elastic scattering. In the approximation that the inelasticity modifies the cross section through the phase space, but not the recoil spectrum, the event rate for the combination of endothermic and exothermic cross sections is equivalent to elastic scattering of the entire abundance of DM with a cross section on protons of

$$\tilde{\sigma}_p = \frac{\sigma_p}{\langle v\rangle}\left(f_2\left\langle\sqrt{v^2-v_\delta^2}\,\Theta(v-v_\delta)\right\rangle + f_3\left\langle\sqrt{v^2+v_\delta^2}\right\rangle\right) \tag{5.9}$$

as in eq. (3.11). The rescaled cross section $\tilde{\sigma}_p$ is shown in figure 8 for several values of the gauge boson masses for the two-Higgs-triplet model. Also shown are the experimental limits, rescaled by $(Z/A)^2$ because the DM couples only to charge in our models. Dark matter

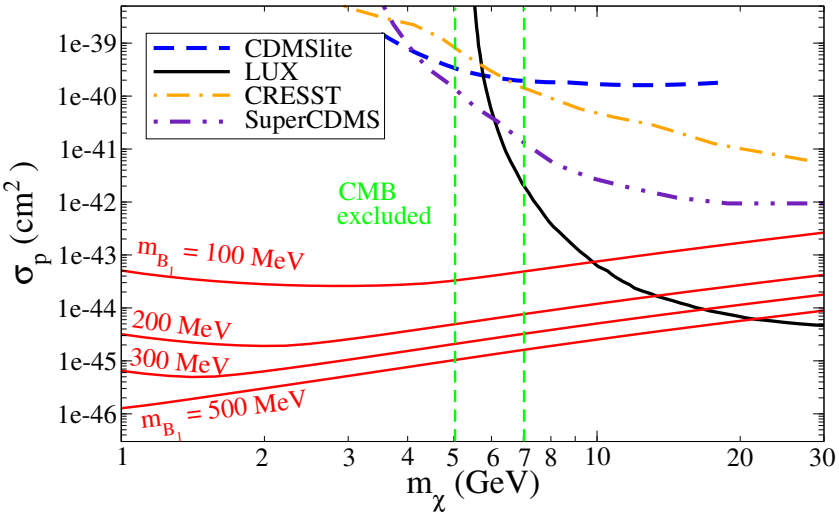

Figure 8. Cross section of triplet DM on protons, assuming ϵ chosen as in (5.6) to produce the X-ray line by long-lived excited DM decay, as well as the thermal relic value for α_g, eq. (3.2). Each theoretically predicted curve is labeled by the B_1 gauge boson mass, assuming a dark Higgs sector with two triplets. As a function of m_{B_1}, the σ_p curve reaches a minimum around $m_{B_1} = 500$ MeV, and increases slightly for larger m_{B_1}. Vertical dashed lines indicate CMB lower limit on M_χ from annihilations, depending upon whether $M_{\chi_1} > M_{\chi_2}$ (right line) or $M_{\chi_1} < M_{\chi_2}$ (left line).

masses of $M_\chi \lesssim 10$ GeV are allowed for $m_{B_1} = 100$ MeV, while larger M_χ is allowed as m_{B_1} increases. However, this dependence on m_{B_1} is not monotonic, due to the factor $F_t(r_2, r_3)^{-2}$ in (5.8) and the relations (5.7) between the gauge boson masses; in fact the growth in the allowed value of M_χ saturates near the $m_{B_1} = 500$ MeV curve shown, so that higher values than $M_\chi \sim 20$ GeV are not allowed by the LUX constraint. For the model with one triplet and one doublet Higgs field on the other hand, the dependence on m_{B_1} is monotonic, and for $m_{B_1} > 300$ MeV the predicted cross sections fall below the current LUX limit, as shown in figure 9.

Like their doublet DM model counterpart, these models of decaying triplet DM are potentially constrained by the CMB. Apart from the slightly different fractional abundance f_x of excited DM in the two models, the decay rate is the same, so the CMB bounds from decays are robustly satisfied, as in figure 6. However, there are related CMB constraints on DM annihilations into SM particles that apply for the triplet model, since it is a symmetric DM candidate. Due to the nonabelian structure of the DM sector, the effective annihilation cross section does not take the canonical relic density value in the late universe. In appendix B we adapt the limits of ref. [98] to this model and find that it must satisfy $M_\chi \gtrsim 5$ GeV (if $M_{\chi_1} < M_{\chi_2}$) or $M_\chi \gtrsim 7$ GeV ($M_{\chi_2} < M_{\chi_1}$), depending on the gauge boson masses, through both the mass splittings and primordial relative abundances. These constraints are compatible with limits on the DM mass from direct detection experiments for gauge boson masses $m_{B_1} \gtrsim 100$ MeV and offer the possibility of detection as CMB limits improve.

5.3 Triplet XDM

We next consider the scenario where triplet DM undergoes collisional excitation followed by fast decays to give the 3.5 keV line. In this case the kinetic mixing is large enough so that

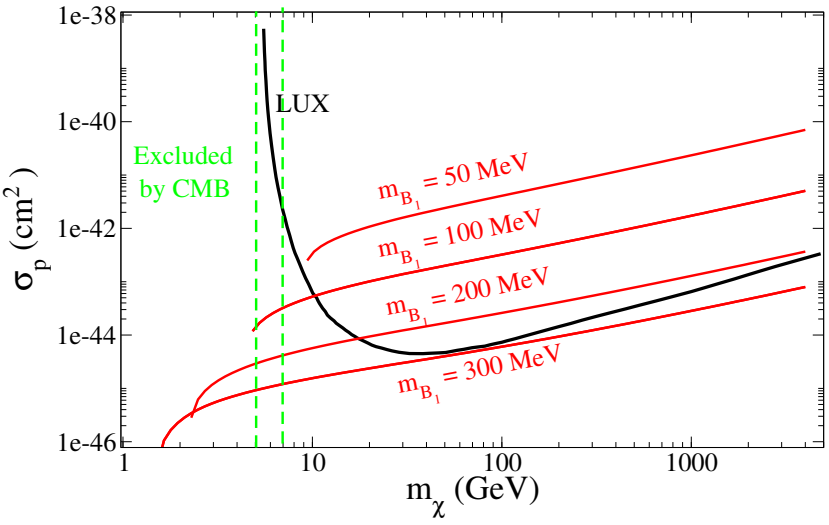

Figure 9. Like figure 8 but for a dark Higgs sector of one triplet and one doublet.

the primordial component of the excited DM state χ_3 has decayed, and is only repopulated by collisional excitation. As discussed in section 4.2, CMB constraints required the lifetime to be less than $\sim 10^{12}$ s. This requires

$$\epsilon \gtrsim 3.8 \times 10^{-9} \frac{(M_\chi/10\text{ GeV})}{F_t(r_2, r_3)\,\alpha_g^{3/2}} = (1.9 \times 10^{-3}) \left(\frac{10\text{ GeV}}{M_\chi}\right)^{1/2} \frac{1}{F_t(r_2, r_3)}, \tag{5.10}$$

with the latter equality representing the bound for thermal relic DM.

We next consider the rate of upscattering needed to populate χ_3 for XDM-like production of the X-ray signal. Suppose first that the entire signal is produced by collisional excitation of a single DM state χ_g, which could be either χ_1 or χ_2, as both are stable in the models we consider. Taking the lower value from equation (2.9), we find that that the gauge boson mediating the upscattering $\chi_g\chi_g \to \chi_3\chi_3$ has mass

$$m_B \cong (3\text{ GeV}) \left(\frac{\alpha_g f_g}{0.33}\right)^{1/2} \left(\frac{v_t\gamma}{1300\text{ km/s}}\right)^{1/4}, \tag{5.11}$$

$$\cong (37\text{ MeV}) \left(\frac{f_g}{0.33}\right)^{1/2} \left(\frac{M_\chi}{10\text{ GeV}}\right)^{1/2} \left(\frac{v_t\gamma}{1300\text{ km/s}}\right)^{1/4} \tag{5.12}$$

where the second line assumes the thermal relic value of the gauge coupling. If we consider excitation of χ_2 DM, then $f_g \sim 2/3$ because of the early universe decays $\chi_3 \to \chi_2\gamma$. This gives a gauge boson mass $m_{B_1} \sim 50$ MeV, very similar to the mass difference needed to account for the 3.55 keV DM mass splitting. It is also possible that $\chi_1\chi_1 \to \chi_3\chi_3$ scattering produces the X-ray signal, either as the dominant contribution or along with $\chi_2\chi_2 \to \chi_3\chi_3$ scattering. In this case, it is m_{B_2} that is $\gtrsim 37$ MeV, and m_{B_1} can be somewhat higher. It is worth noting that the mass gap δM_{13} may be either larger or smaller than 3.55 keV, so the relative contribution of each type of upscattering differs in M31 and the Perseus cluster. However, these corrections are all of order unity.

Direct detection imposes stringent constraints on these models for DM masses of order $M_\chi = 10$ GeV. Using (5.10) and (5.11), we find that the cross section for DM-proton inelastic

scattering is

$$\sigma_p \gtrsim \frac{2.2\times10^{-47}\ \mathrm{cm}^2}{\alpha_g^4\, F_t(r_2,r_3)^2}\left(1+\frac{m_p}{M_\chi}\right)^{-2}\left(\frac{M_\chi}{10\ \mathrm{GeV}}\right)^2\left(\frac{0.33}{f_g}\right)^2\left(\frac{1300\ \mathrm{km/s}}{v_t\gamma}\right), \tag{5.13}$$

where $v_t\gamma$ is the appropriate value for the Perseus cluster. For comparison to elastic scattering experiments, we rescale the cross section as in equation (5.9) with $f_3 = 0$. With nonthermal DM production, α_g as small as 0.01 and somewhat lighter DM masses 3-5 GeV avoid current direct detection constraints.

Using the thermal relic value for α_g yields a much stronger constraint

$$\sigma_p \gtrsim \frac{4\times10^{-32}\ \mathrm{cm}^2}{F_t(r_2,r_3)^2}\left(1+\frac{m_p}{M_\chi}\right)^{-2}\left(\frac{10\ \mathrm{GeV}}{M_\chi}\right)^2\left(\frac{0.33}{f_g}\right)^2\left(\frac{1300\ \mathrm{km/s}}{v_t\gamma}\right), \tag{5.14}$$

which forces $M_\chi \sim 1$ GeV, below the sensitivity of current direct detection experiments. At these low masses, kinematic suppression of the scattering rate due to the inelasticity becomes a strong effect and is worth studying in more detail as more sensitive direct detection experiments come online. This cross section can be reduced slightly if m_{B_1} is somewhat larger than (5.12) but only by about an order of magnitude, which does not by itself remove this constraint.

However, CMB constraints on DM annihilation will essentially rule out these models in combination with direct detection constraints. As described in appendix B, we find that CMB bounds require $M_\chi > 6$ GeV for triplet XDM. This would only be consistent with the direct detection constraints on the thermal WIMP model discussed above if some combination of parameter choices could drastically reduce the direct detection cross section. Nonthermal DM production with larger α_g will reduce the DM-proton scattering cross section given in equation (5.13) at the cost of increasing the annihilation cross section and therefore tightening the CMB constraint. We would therefore have to consider replacing the Majorana DM with Dirac DM and taking an asymmetric DM model in order to make triplet XDM a viable option.

6 Discussion

Nonabelian dark matter models with a light kinetically mixed gauge boson can naturally incorporate the small mass splitting and coupling to photons that would be needed for decays of an excited DM state to explain the 3.5 keV X-ray line. We find that the DM mass should be in the approximate range $1 - 10$ GeV, with the possibility of larger masses for decaying triplet DM (depending on the dark Higgs content; see fig. 9), and the gauge bosons masses should be $\lesssim 1$ GeV. There are good prospects for direct detection of the DM by its scattering on protons. Moreover the kinetic mixing parameter and gauge boson masses typically fall into regions that will be probed by the HPS experiment within the next year.

Generally, a given model can exist in either of two regimes, where the excited state is metastable and primordial, or else having a shorter lifetime and produced through inelastic scatterings (XDM mechanism). Models of the former kind easily satisfy CMB constraints from injection of electromagnetic energy during recombination, but the latter kind are more strongly constrained by the CMB, needing much larger values of the kinetic mixing in order to decay well before recombination. For the doublet XDM model, it requires taking M_χ below a few GeV to evade direct detection, while for the triplet model, since it is a symmetric dark

matter candidate, this loophole is blocked by CMB constraints on annihilations, so that the XDM version of the triplet model is ruled out (though asymmetric Dirac triplet DM could be made acceptable).

In previous literature, nonabelian DM models were explored as a means of explaining the anomalous 511 keV gamma ray line from the galactic center [70]. One could be tempted to try to combine this and the 3.5 keV line in a triplet DM model where there are two mass splittings corresponding to these energies. We find (details not described here) that although it is possible to arrange for the desired splittings, the relative strengths of the two lines cannot be correctly reproduced in these models with small multiplets because the transition with the larger energy has too big a rate relative to the smaller one, due to the larger phase space for the decays.

Similarly, one may wonder whether our model could simultaneously explain the GeV-scale galactic center excess [18, 19], since general models of DM interacting through kinetically mixed vector mediators have been shown to give a good fit to the data [99, 100]. However the best fit region is for $m_\chi \sim m_B \sim 30$ GeV, which is generally incompatible with the parameters we have identified for the X-ray line. For example, eq. (4.1) for the slow-decaying doublet model implies $\epsilon \sim 10^{-5}/\alpha_g^{3/2}$, giving a cross section on protons of $\sigma_p \gtrsim 3\times 10^{-44}\,\mathrm{cm}^2$ that is firmly excluded by LUX. More recently it has been pointed out that inclusion of inverse Compton scattering and brehmsstrahlung contributions can lead to lower best-fit values $M_\chi \sim 10$ GeV consistent with leptonic final states [101, 102]. These authors do not consider the 4-lepton final states that would arise from pairs of gauge bosons, so we cannot draw any direct conclusions from their work, but if for example $m_B = 3$ GeV rather than ~ 30 GeV, this would reduce ϵ by a factor of 100 and σ_p by a factor of 10^4, safely below current direct detection limits. We leave this interesting question for a separate study.

The 3.5 keV line awaits confirmation by higher-statistics observations. So far the only study to cast doubt on the observation is a negative search for the line in our own galactic center [103]; however the conclusions depend upon uncertain assumptions about the shape of the dark matter halo profile in this region. In our study we have pointed out a possible way of discriminating between and XDM and decaying models for the X-ray line: since the XDM mechanism depends upon the DM velocity dispersion through $\langle\sigma v_{\rm rel}\rangle$, one could expect that the line strength will be relatively stronger from galactic clusters with higher $v_{\rm rel}$ than from individual galaxies like M31 (see also [54]). We quantified this for the predicted signal in fig. 2. There is already a hint of such an effect in the present determinations of the required value of $\langle\sigma v_{\rm rel}\rangle$. It will be interesting to see whether it persists as the observations improve.

Acknowledgment. We thank Wei Xue for helpful discussions concerning the galactic center gamma ray excess. Our work is supported by the Natural Sciences and Engineering Research Council (NSERC) of Canada.

A Magnetic moments

We derive the one-loop results for the transition magnetic moments of the dark matter multiplets, starting with the case of SU(2) triplet DM. In a constant external magnetic field, the triple-gauge interaction from the kinetic mixing operator takes the form $\epsilon g F_{\mu\nu} B_2^\mu B_3^\nu$. In the case of equal gauge boson masses, the effective operator involving $F_{\mu\nu}$ can be written as

$$\epsilon g^3 \bar{u}_2(p) \left[\int \frac{d^4\ell}{(2\pi)^4} \frac{\gamma_\mu(\not{\ell} + M_\chi)\gamma_\nu}{(\ell^2 + 2\ell\cdot p)(\ell^2 - m_B^2 + i\epsilon)^2}\right] u_3(p)\, F^{\mu\nu} \tag{A.1}$$

setting the momentum of the constant field to zero and ignoring the small DM mass splittings. p is the external fermion momentum which is taken to be on shell, $p^2 = M_\chi^2$. The term in brackets becomes

$$\frac{i}{16\pi^2}\int_0^1 dx\,(1-x)\frac{\gamma_\mu(\not{p}(1-x)+M_\chi)\gamma_\nu}{x^2\,M_\chi^2+(1-x)\mu^2} \tag{A.2}$$

after doing the momentum integral. By anticommuting half of the $\not{p}$ term through each gamma matrix and using the Dirac equation, we find that $\not{p}\to -m$ plus terms that are symmetric under $\mu\leftrightarrow\nu$, hence vanish under contraction with the field strength. The x integral can be done, resulting in the transition magnetic moment

$$\mu_\times = \frac{\epsilon g^3}{16\pi^2\,M_\chi}F_t(m_B^2/M_\chi^2) \tag{A.3}$$

where

$$F_t(r) = \frac{1-r}{2}\ln\frac{1}{r} - 1 + \frac{3-r}{\sqrt{4/r-1}}\tan^{-1}\sqrt{4/r-1} \tag{A.4}$$

It has leading behavior $\frac{1}{2}\ln(1/r)$ at small r. For the case of two different gauge boson masses in the loop, we define $r_i = m_{B_i}^2/M_\chi^2$ and obtain in place of (A.2)

$$\frac{i}{16\pi^2}\int_0^1 dx\int_0^{1-x} dy\,\frac{\gamma_\mu(\not{p}(1-x)+M_\chi)\gamma_\nu}{x^2\,M_\chi^2+ym_{B_1}^2+(1-x-y)m_{B_2}^2} \tag{A.5}$$

leading to

$$\begin{aligned}F_t(r_1,r_2) = {}& \frac{\sqrt{(4-r_1)}\,r_1^{3/2}\tan^{-1}\sqrt{4/r_1-1}-\sqrt{(4-r_2)}\,r_2^{3/2}\tan^{-1}\sqrt{4/r_2-1}}{2(r_1-r_2)}\\ &+\frac{(r_1^2-2r_1)\ln r_1-(r_2^2-2r_2)\ln r_2}{4(r_1-r_2)}-\frac{1}{2}\end{aligned} \tag{A.6}$$

One can show that (A.6) reduces to (A.4) in the limit $r_1\to r_2 = r$.

The above results can be generalized to other DM representations of SU(N) by including the group theory factor

$$G = f^{\hat{a}bc}T_{2i}^c T_{i1}^b \tag{A.7}$$

assuming that the DM mass eigenstates labeled $1,2$ correspond to the generators T_{i1}^b, T_{2i}^c respectively, and $\hat{a}$ denotes the gauge boson that kinetically mixes with the photon. One must sum over gauge bosons with masses m_{B_b} and m_{B_c} as well as the internal DM state with mass M_{χ_i}. If the mass differences can be neglected in the loop integral (as fig. 3 shows is often a good approximation) then the sums over i,b,c can be done directly in (A.7), giving

$$G = \frac{i}{2}C_2(A)T_{21}^{\hat{a}} \tag{A.8}$$

where $C(A)$ is the quadratic Casimir invariant of the adjoint representation. The multiplicative correction factor (A.8) is unity for the triplet model in SU(2).

In the SU(2) doublet DM model, the transition magnetic moment gets nearly canceling contributions from both χ_1 and χ_2 in the loop, such that the result is suppressed by δM_χ.

One must therefore be more careful in distinguishing the incoming and outgoing fermion momenta $p_{1,2}$, and keeping the dependence on the photon momentum $q = p_1 - p_2$. The induced operator is

$$\epsilon g^3 \bar{u}_1(p_1) \left[\int \frac{d^4\ell}{(2\pi)^4} \frac{\gamma_\mu(\not{\ell} + \not{p} + m_1)\gamma_\nu}{((\ell+p)^2 - m_1^2)((\ell - q/2)^2 + m_B^2)((\ell + q/2)^2 + m_B^2)} \right] u_2(p_2)\, F^{\mu\nu}(q) - \{m_1 \to m_2\} \tag{A.9}$$

where $p = \frac{1}{2}(p_1 + p_2)$. Introducing Feynman parameters x and y for the two gauge boson propagators (hence $(1 - x - y)$ for the fermion) we find the result

$$\mu_\times = \frac{\epsilon g^3}{16\pi^2} \frac{\delta M_\chi}{M_\chi^2} F_d(r) \tag{A.10}$$

to leading order in δM_χ for the transition magnetic moment, with $r = m_B^2/M_\chi^2$ and

$$\begin{aligned} F_d(r) &= \int_0^1 dx \int_0^{1-x} dy \, \frac{(1-x-y) + r(x+y)}{\left((1-x-y)^2 + r(x+y)\right)^2} \\ &= \frac{2-r}{r(4-r)} + 2\frac{\tan^{-1}\sqrt{4/r - 1}}{\sqrt{r}(4-r)^{3/2}} \end{aligned} \tag{A.11}$$

which has leading behavior $1/(2r)$ at small r. This implies that for $m_B \ll M_\chi$, the transition moment in the doublet model goes like $\delta M_\chi / m_B^2$ instead of $1/M_\chi$.

B CMB bounds from DM annihilation

In this appendix, we give details concerning the constraints on the mass M_χ of triplet DM models described in section 5 coming from the cosmic microwave background. Combined limits from Planck, WMAP9, ACT, and SPT (plus low-redshift data) constrain DM with canonical annihilation cross section $\sigma v = 3 \times 10^{-26}$ cm^3/s to have mass $M_\chi > (26\text{ GeV}) f$, where f is the effective energy deposition efficiency [98]. For "XDM-like" annihilation processes $\chi\chi \to BB$ followed by $B_1 \to e^+e^-$, the efficiency is $f = 0.67$ for DM masses near 10 GeV [98]. This efficiency is larger than for $B_1 \to 2\mu$ or $B_1 \to 2\pi$ decay channels when they are allowed. Since we are mostly concerned with lighter gauge boson masses, we conservatively take $f = 0.67$. However, the constraints we find below are loosened somewhat for $m_{B_1} > 2m_\mu$.

We account for several additional effects in our models. First, as described in section 3, we use the adjusted value of the thermal relic cross section, which is approximately 0.7 of the canonical value at DM mass of 10 GeV but increases to the canonical value at 5 GeV DM mass.

There are other effects due to the nonabelian structure of the dark sector. The energy deposition efficiency is reduced by the fact that the relic abundance is determined by the total annihilation cross section for $\chi\chi \to BB$, but only B_1 gauge bosons decay into SM particles. Therefore, we count only annihilations with B_1 final particles toward the energy deposition efficiency (weighting final states with a single B_1 with 1/2). Finally, the relative abundances of the DM species differ in the present universe relative to those at chemical freeze out due to kinetic equilibration at lower temperatures during the Big Bang. As a result of these

two effects, the effective average annihilation cross section is modified in the late universe compared to the canonical value. As given in the appendix of [70], the color- and spin-averaged and summed square amplitude for the total annihilation cross section (assuming equal abundances for each "color," or DM state) is $|\mathcal{M}_{tot}|^2 = 25g^4/6$, not including any overcounting or symmetry factors for identical initial or final particles. This is composed of amplitudes for two types of processes, $\mathcal{M}_{12\to12}$, which involves t- and s-channel diagrams, and $\mathcal{M}_{22\to11}$, with t- and u-channel parts. As we approximate vanishing gauge boson masses, the amplitudes are equal when gauge indices are permuted. The effective squared amplitude at late times, including all permutations and weighting $\mathcal{M}_{12\to12}$ contributions by 1/2, is

$$|\mathcal{M}_{eff}|^2 = \frac{4}{2} f_1 f_2 |\mathcal{M}_{12\to12}|^2 + \frac{4}{2} f_1 f_3 |\mathcal{M}_{13\to13}|^2 + f_2^2 |\mathcal{M}_{22\to11}|^2 + f_3^2 |\mathcal{M}_{33\to11}|^2 \quad \text{(B.1)}$$

$$= \left[\frac{9}{2} f_1 (1 - f_1) + 4(f_2^2 + f_3^2)\right] g^4. \quad \text{(B.2)}$$

We therefore rescale the energy deposition efficiency by $|\mathcal{M}_{eff}|^2/|\mathcal{M}_{tot}|^2$.

In the decaying triplet model, the fractional relic abundances f_a are set by kinetic freezeout in the Big Bang. For fiducial values $f_1 = f_2 = f_3 = 1/3$, we find the bound $M_\chi \gtrsim 6$ GeV. For specific values of the mass splittings and gauge boson masses, the relative abundances change somewhat; representative abundances are $f_1 = 0.66$, $f_2 = 0.23$, $f_3 = 0.11$ if $M_{\chi_1} < M_{\chi_2}$ or $f_1 = 0.23$, $f_2 = 0.66$, $f_3 = 0.11$ if $M_{\chi_2} < M_{\chi_1}$. These lead to CMB bounds of 5 GeV and 7 GeV respectively.

In the XDM model, the primordial χ_3 population decays early, adding to the χ_2 abundance. Therefore, the three cases described above have $f_1 = 1/3$, $f_2 = 2/3$, $f_3 = 0$ with $M_\chi > 8$ GeV, $f_1 = 0.66$, $f_2 = 0.34$, $f_3 = 0$ with $M_\chi > 6$ GeV, and $f_1 = 0.23$, $f_2 = 0.77$, $f_3 = 0$ with $M_\chi > 9$ GeV. These values are inconsistent with the direct detection bounds for the XDM model.

References

[1] **DAMA Collaboration** Collaboration, R. Bernabei *et. al.*, *First results from DAMA/LIBRA and the combined results with DAMA/NaI*, *Eur.Phys.J.* **C56** (2008) 333–355, [0804.2741].

[2] G. Angloher, M. Bauer, I. Bavykina, A. Bento, C. Bucci, *et. al.*, *Results from 730 kg days of the CRESST-II Dark Matter Search*, 1109.0702.

[3] C. Aalseth, P. Barbeau, J. Colaresi, J. Collar, J. Diaz Leon, *et. al.*, *Search for an Annual Modulation in a P-type Point Contact Germanium Dark Matter Detector*, *Phys.Rev.Lett.* **107** (2011) 141301, [1106.0650].

[4] **CoGeNT collaboration** Collaboration, C. Aalseth *et. al.*, *Results from a Search for Light-Mass Dark Matter with a P-type Point Contact Germanium Detector*, *Phys.Rev.Lett.* **106** (2011) 131301, [1002.4703].

[5] **CoGeNT Collaboration** Collaboration, C. Aalseth *et. al.*, *Search for An Annual Modulation in Three Years of CoGeNT Dark Matter Detector Data*, 1401.3295.

[6] **CDMS Collaboration** Collaboration, R. Agnese *et. al.*, *Silicon Detector Dark Matter Results from the Final Exposure of CDMS II*, *Phys.Rev.Lett.* **111** (2013) 251301, [1304.4279].

[7] **XENON10 Collaboration** Collaboration, J. Angle *et. al.*, *A search for light dark matter in XENON10 data*, *Phys.Rev.Lett.* **107** (2011) 051301, [1104.3088].

[8] **XENON100 Collaboration** Collaboration, E. Aprile *et. al.*, *Analysis of the XENON100 Dark Matter Search Data*, *Astropart.Phys.* **54** (2014) 11–24, [1207.3458].

[9] **XENON100 Collaboration** Collaboration, E. Aprile *et. al.*, *Dark Matter Results from 225 Live Days of XENON100 Data*, *Phys.Rev.Lett.* **109** (2012) 181301, [1207.5988].

[10] **LUX Collaboration** Collaboration, D. Akerib *et. al.*, *First results from the LUX dark matter experiment at the Sanford Underground Research Facility*, *Phys.Rev.Lett.* **112** (2014) 091303, [1310.8214].

[11] **SuperCDMSSoudan Collaboration** Collaboration, R. Agnese *et. al.*, *CDMSlite: A Search for Low-Mass WIMPs using Voltage-Assisted Calorimetric Ionization Detection in the SuperCDMS Experiment*, *Phys.Rev.Lett.* **112** (2014) 041302, [1309.3259].

[12] **PAMELA Collaboration** Collaboration, O. Adriani *et. al.*, *An anomalous positron abundance in cosmic rays with energies 1.5-100 GeV*, *Nature* **458** (2009) 607–609, [0810.4995].

[13] **HEAT Collaboration** Collaboration, S. Barwick *et. al.*, *Measurements of the cosmic ray positron fraction from 1-GeV to 50-GeV*, *Astrophys.J.* **482** (1997) L191–L194, [astro-ph/9703192].

[14] J. Chang, J. Adams, H. Ahn, G. Bashindzhagyan, M. Christl, *et. al.*, *An excess of cosmic ray electrons at energies of 300-800 GeV*, *Nature* **456** (2008) 362–365.

[15] **PPB-BETS Collaboration** Collaboration, S. Torii *et. al.*, *High-energy electron observations by PPB-BETS flight in Antarctica*, 0809.0760.

[16] T. Bringmann, X. Huang, A. Ibarra, S. Vogl, and C. Weniger, *Fermi LAT Search for Internal Bremsstrahlung Signatures from Dark Matter Annihilation*, *JCAP* **1207** (2012) 054, [1203.1312].

[17] C. Weniger, *A Tentative Gamma-Ray Line from Dark Matter Annihilation at the Fermi Large Area Telescope*, *JCAP* **1208** (2012) 007, [1204.2797].

[18] D. Hooper and T. Linden, *On The Origin Of The Gamma Rays From The Galactic Center*, *Phys.Rev.* **D84** (2011) 123005, [1110.0006].

[19] K. N. Abazajian and M. Kaplinghat, *Detection of a Gamma-Ray Source in the Galactic Center Consistent with Extended Emission from Dark Matter Annihilation and Concentrated Astrophysical Emission*, *Phys.Rev.* **D86** (2012) 083511, [1207.6047].

[20] D. Hooper and L. Goodenough, *Dark Matter Annihilation in The Galactic Center As Seen by the Fermi Gamma Ray Space Telescope*, *Phys.Lett.* **B697** (2011) 412–428, [1010.2752].

[21] L. Goodenough and D. Hooper, *Possible Evidence For Dark Matter Annihilation In The Inner Milky Way From The Fermi Gamma Ray Space Telescope*, 0910.2998.

[22] W. N. Johnson, III, F. R. Harnden, Jr., and R. C. Haymes, *The Spectrum of Low-Energy Gamma Radiation from the Galactic-Center Region.*, *Astrophys.J.Lett.* **172** (Feb., 1972) L1.

[23] M. Leventhal, C. J. MacCallum, and P. D. Stang, *Detection of 511 keV positron annihilation radiation from the galactic center direction*, *Astrophys.J.Lett.* **225** (Oct., 1978) L11–L14.

[24] E. Bulbul, M. Markevitch, A. Foster, R. K. Smith, M. Loewenstein, *et. al.*, *Detection of An Unidentified Emission Line in the Stacked X-ray spectrum of Galaxy Clusters*, 1402.2301.

[25] A. Boyarsky, O. Ruchayskiy, D. Iakubovskyi, and J. Franse, *An unidentified line in X-ray spectra of the Andromeda galaxy and Perseus galaxy cluster*, 1402.4119.

[26] H. Ishida, K. S. Jeong, and F. Takahashi, *7 keV sterile neutrino dark matter from split flavor mechanism*, *Phys.Lett.* **B732** (2014) 196–200, [1402.5837].

[27] K. N. Abazajian, *Resonantly-Produced 7 keV Sterile Neutrino Dark Matter Models and the Properties of Milky Way Satellites*, *Phys.Rev.Lett.* **112** (2014) 161303, [1403.0954].

[28] S. Baek and H. Okada, *7 keV Dark Matter as X-ray Line Signal in Radiative Neutrino Model*, 1403.1710.

[29] B. Shuve and I. Yavin, *A Dark Matter Progenitor: Light Vector Boson Decay into (Sterile) Neutrinos*, *Phys.Rev.* **D89** (2014) 113004, [1403.2727].

[30] T. Tsuyuki, *Neutrino masses, leptogenesis, and sterile neutrino dark matter*, 1403.5053.

[31] F. Bezrukov and D. Gorbunov, *Relic Gravity Waves and 7 keV Dark Matter from a GeV scale inflaton*, 1403.4638.

[32] K. P. Modak, *3.5 keV X-ray Line Signal from Decay of Right-Handed Neutrino due to Transition Magnetic Moment*, 1404.3676.

[33] D. J. Robinson and Y. Tsai, *A Dynamical Framework for KeV Dirac Neutrino Warm Dark Matter*, 1404.7118.

[34] S. Chakraborty, D. K. Ghosh, and S. Roy, *7 keV Sterile neutrino dark matter in $U(1)_R-$ lepton number model*, 1405.6967.

[35] N. Haba, H. Ishida, and R. Takahashi, *ν_R dark matter-philic Higgs for 3.5 keV X-ray signal*, 1407.6827.

[36] T. Higaki, K. S. Jeong, and F. Takahashi, *The 7 keV axion dark matter and the X-ray line signal*, *Phys.Lett.* **B733** (2014) 25–31, [1402.6965].

[37] J. Jaeckel, J. Redondo, and A. Ringwald, *A 3.55 keV hint for decaying axion-like particle dark matter*, *Phys.Rev.* **D89** (2014) 103511, [1402.7335].

[38] H. M. Lee, S. C. Park, and W.-I. Park, *Cluster X-ray line at* 3.5 keV *from axion-like dark matter*, 1403.0865.

[39] M. Cicoli, J. P. Conlon, M. C. D. Marsh, and M. Rummel, *A 3.55 keV Photon Line and its Morphology from a 3.55 keV ALP Line*, 1403.2370.

[40] A. Dias, A. Machado, C. Nishi, A. Ringwald, and P. Vaudrevange, *The Quest for an Intermediate-Scale Accidental Axion and Further ALPs*, *JHEP* **1406** (2014) 037, [1403.5760].

[41] J.-C. Park, S. C. Park, and K. Kong, *X-ray line signal from 7 keV axino dark matter decay*, *Phys.Lett.* **B733** (2014) 217–220, [1403.1536].

[42] K.-Y. Choi and O. Seto, *X-ray line signal from decaying axino warm dark matter*, *Phys.Lett.* **B735** (2014) 92, [1403.1782].

[43] S. P. Liew, *Axino dark matter in light of an anomalous X-ray line*, *JCAP* **1405** (2014) 044, [1403.6621].

[44] R. Krall, M. Reece, and T. Roxlo, *Effective field theory and keV lines from dark matter*, 1403.1240.

[45] K. Nakayama, F. Takahashi, and T. T. Yanagida, *The 3.5 keV X-ray line signal from decaying moduli with low cutoff scale*, 1403.1733.

[46] K. Nakayama, F. Takahashi, and T. T. Yanagida, *Anomaly-free flavor models for Nambu-Goldstone bosons and the 3.5 keV X-ray line signal*, *Phys.Lett.* **B734** (2014) 178–182, [1403.7390].

[47] C. Kolda and J. Unwin, *X-ray lines from R-parity violating decays of keV sparticles*, 1403.5580.

[48] N. E. Bomark and L. Roszkowski, *The 3.5 keV X-ray line from decaying gravitino dark matter*, 1403.6503.

[49] S. Demidov and D. Gorbunov, *SUSY in the sky or keV signature of sub-GeV gravitino dark matter*, 1404.1339.

[50] B. Dutta, I. Gogoladze, R. Khalid, and Q. Shafi, *3.5 keV X-ray line and R-Parity Conserving Supersymmetry*, 1407.0863.

[51] F. S. Queiroz and K. Sinha, *The Poker Face of the Majoron Dark Matter Model: LUX to keV Line*, *Phys.Lett.* **B735** (2014) 69–74, [1404.1400].

[52] E. Dudas, L. Heurtier, and Y. Mambrini, *Generating X-ray lines from annihilating dark matter*, 1404.1927.

[53] K. Babu and R. N. Mohapatra, *7 keV Scalar Dark Matter and the Anomalous Galactic X-ray Spectrum*, *Phys.Rev.* **D89** (2014) 115011, [1404.2220].

[54] D. P. Finkbeiner and N. Weiner, *An X-Ray Line from eXciting Dark Matter*, 1402.6671.

[55] C. E. Aisati, T. Hambye, and T. Scarna, *Can a millicharged dark matter particle emit an observable gamma-ray line?*, 1403.1280.

[56] M. T. Frandsen, F. Sannino, I. M. Shoemaker, and O. Svendsen, *X-ray Lines from Dark Matter: The Good, The Bad, and The Unlikely*, *JCAP* **1405** (2014) 033, [1403.1570].

[57] R. Allahverdi, B. Dutta, and Y. Gao, *keV Photon Emission from Light Nonthermal Dark Matter*, 1403.5717.

[58] J. M. Cline, Y. Farzan, Z. Liu, G. D. Moore, and W. Xue, *3.5 keV X-rays as the "21 cm line" of dark atoms, and a link to light sterile neutrinos*, *Phys.Rev.* **D89** (2014) 121302, [1404.3729].

[59] H. Okada and T. Toma, *The 3.55 keV X-ray Line Signal from Excited Dark Matter in Radiative Neutrino Model*, 1404.4795.

[60] H. M. Lee, *Magnetic dark matter for the X-ray line at 3.55 keV*, 1404.5446.

[61] D. P. Finkbeiner and N. Weiner, *Exciting Dark Matter and the INTEGRAL/SPI 511 keV signal*, *Phys.Rev.* **D76** (2007) 083519, [astro-ph/0702587].

[62] M. Pospelov and A. Ritz, *The galactic 511 keV line from electroweak scale WIMPs*, *Phys.Lett.* **B651** (2007) 208–215, [hep-ph/0703128].

[63] D. P. Finkbeiner, N. Padmanabhan, and N. Weiner, *CMB and 21-cm Signals for Dark Matter with a Long-Lived Excited State*, *Phys.Rev.* **D78** (2008) 063530, [0805.3531].

[64] N. Arkani-Hamed, D. P. Finkbeiner, T. R. Slatyer, and N. Weiner, *A Theory of Dark Matter*, *Phys.Rev.* **D79** (2009) 015014, [0810.0713].

[65] F. Chen, J. M. Cline, and A. R. Frey, *A New twist on excited dark matter: Implications for INTEGRAL, PAMELA/ATIC/PPB-BETS, DAMA*, *Phys.Rev.* **D79** (2009) 063530, [0901.4327].

[66] D. P. Finkbeiner, T. R. Slatyer, N. Weiner, and I. Yavin, *PAMELA, DAMA, INTEGRAL and Signatures of Metastable Excited WIMPs*, *JCAP* **0909** (2009) 037, [0903.1037].

[67] B. Batell, M. Pospelov, and A. Ritz, *Direct Detection of Multi-component Secluded WIMPs*, *Phys.Rev.* **D79** (2009) 115019, [0903.3396].

[68] F. Chen, J. M. Cline, and A. R. Frey, *Nonabelian dark matter: Models and constraints*, *Phys.Rev.* **D80** (2009) 083516, [0907.4746].

[69] F. Chen, J. M. Cline, A. Fradette, A. R. Frey, and C. Rabideau, *Exciting dark matter in the galactic center*, *Phys.Rev.* **D81** (2010) 043523, [0911.2222].

[70] J. M. Cline, A. R. Frey, and F. Chen, *Metastable dark matter mechanisms for INTEGRAL 511 keV γ rays and DAMA/CoGeNT events*, *Phys.Rev.* **D83** (2011) 083511, [1008.1784].

[71] A. C. Vincent, P. Martin, and J. M. Cline, *Interacting dark matter contribution to the Galactic 511 keV gamma ray emission: constraining the morphology with INTEGRAL/SPI observations*, *JCAP* **1204** (2012) 022, [1201.0997].

[72] J. M. Cline and A. R. Frey, *Abelian dark matter models for 511 keV gamma rays and direct detection*, *Annalen Phys.* **524** (2012) 579–590, [1204.1965].

[73] Y. Bai, M. Su, and Y. Zhao, *Dichromatic Dark Matter*, 1212.0864.

[74] A. R. Frey and N. B. Reid, *Cosmic microwave background constraints on dark matter models of the Galactic center 511 keV signal*, *Phys.Rev.* **D87** (2013), no. 10 103508, [1301.0819].

[75] S. D. Thomas and J. D. Wells, *Phenomenology of Massive Vectorlike Doublet Leptons*, *Phys.Rev.Lett.* **81** (1998) 34–37, [hep-ph/9804359].

[76] S. C. Chapman, R. Ibata, G. Lewis, A. Ferguson, M. Irwin, *et. al.*, *A kinematically selected, metal-poor spheroid in the outskirts of m31*, *Astrophys.J.* **653** (2006) 255–266, [astro-ph/0602604].

[77] R. Saglia, M. Fabricius, R. Bender, M. Montalto, C.-H. Lee, *et. al.*, *The old and heavy bulge of M31 I. Kinematics and stellar populations*, 0910.5590.

[78] L. Danese, G. de Zotti, and G. di Tullio, *On velocity dispersions of galaxies in rich clusters*, *Astronomy and Astrophysics* **82** (Feb., 1980) 322–327.

[79] S. M. Kent and W. L. W. Sargent, *The dynamics of rich clusters of galaxies. II - The Perseus cluster*, *Astrophys.J.* **88** (June, 1983) 697–708.

[80] A. Tamm, E. Tempel, P. Tenjes, O. Tihhonova, and T. Tuvikene, *Stellar mass map and dark matter distribution in M31*, 1208.5712.

[81] D. H. Weinberg, J. S. Bullock, F. Governato, R. K. de Naray, and A. H. G. Peter, *Cold dark matter: controversies on small scales*, 1306.0913.

[82] M. A. Sanchez-Conde, M. Cannoni, F. Zandanel, M. E. Gomez, and F. Prada, *Dark matter searches with Cherenkov telescopes: nearby dwarf galaxies or local galaxy clusters?*, *JCAP* **1112** (2011) 011, [1104.3530].

[83] J. Aleksić *et al.* (MAGIC Collaboration), *MAGIC Gamma-ray Telescope Observation of the Perseus Cluster of Galaxies: Implications for Cosmic Rays, Dark Matter, and NGC 1275*, *Astrophys.J.* **710** (Feb., 2010) 634–647, [0909.3267].

[84] G. Steigman, B. Dasgupta, and J. F. Beacom, *Precise Relic WIMP Abundance and its Impact on Searches for Dark Matter Annihilation*, *Phys.Rev.* **D86** (2012) 023506, [1204.3622].

[85] E. Del Nobile, G. B. Gelmini, P. Gondolo, and J.-H. Huh, *Direct detection of Light Anapole and Magnetic Dipole DM*, *JCAP* **1406** (2014) 002, [1401.4508].

[86] **HPS** Collaboration, S. Stepanyan, *Heavy photon search experiment at JLAB*, *AIP Conf.Proc.* **1563** (2013) 155–158.

[87] **Collaboration for the SuperCDMS** Collaboration, A. Anderson, *Constraints on Light WIMPs from SuperCDMS*, 1405.4210.

[88] **CRESST Collaboration** Collaboration, G. Angloher *et. al.*, *Results on low mass WIMPs using an upgraded CRESST-II detector*, 1407.3146.

[89] M. Mapelli, A. Ferrara, and E. Pierpaoli, *Impact of dark matter decays and annihilations on reionzation*, *Mon.Not.Roy.Astron.Soc.* **369** (2006) 1719–1724, [astro-ph/0603237].

[90] L. Zhang, X. Chen, M. Kamionkowski, Z.-g. Si, and Z. Zheng, *Constraints on radiative dark-matter decay from the cosmic microwave background*, *Phys.Rev.* **D76** (2007) 061301, [0704.2444].

[91] D. P. Finkbeiner, S. Galli, T. Lin, and T. R. Slatyer, *Searching for Dark Matter in the CMB: A Compact Parameterization of Energy Injection from New Physics*, *Phys.Rev.* **D85** (2012) 043522, [1109.6322].

[92] S. Yeung, M. Chan, and M.-C. Chu, *Cosmic Microwave Background constraints of decaying dark matter particle properties*, *Astrophys.J.* **755** (2012) 108, [1206.4114].

[93] T. R. Slatyer, *Energy Injection And Absorption In The Cosmic Dark Ages*, 1211.0283.

[94] J. M. Cline and P. Scott, *Dark Matter CMB Constraints and Likelihoods for Poor Particle Physicists*, *JCAP* **1303** (2013) 044, [1301.5908].

[95] R. Diamanti, L. Lopez-Honorez, O. Mena, S. Palomares-Ruiz, and A. C. Vincent, *Constraining Dark Matter Late-Time Energy Injection: Decays and P-Wave Annihilations*, *JCAP* **1402** (2014) 017, [1308.2578].

[96] D. E. Morrissey and A. P. Spray, *New Limits on Light Hidden Sectors from Fixed-Target Experiments*, 1402.4817.

[97] J. B. Dent, F. Ferrer, and L. M. Krauss, *Constraints on Light Hidden Sector Gauge Bosons from Supernova Cooling*, 1201.2683.

[98] M. S. Madhavacheril, N. Sehgal, and T. R. Slatyer, *Current Dark Matter Annihilation Constraints from CMB and Low-Redshift Data*, *Phys.Rev.* **D89** (2014) 103508, [1310.3815].

[99] A. Berlin, P. Gratia, D. Hooper, and S. D. McDermott, *Hidden Sector Dark Matter Models for the Galactic Center Gamma-Ray Excess*, 1405.5204.

[100] J. M. Cline, G. Dupuis, Z. Liu, and W. Xue, *The windows for kinetically mixed Z'-mediated dark matter and the galactic center gamma ray excess*, 1405.7691.

[101] T. Lacroix, C. Boehm, and J. Silk, *Fitting the Fermi-LAT GeV excess: on the importance of including the propagation of electrons from dark matter*, 1403.1987.

[102] M. Cirelli, D. Gaggero, G. Giesen, M. Taoso, and A. Urbano, *Antiproton constraints on the GeV gamma-ray excess: a comprehensive analysis*, 1407.2173.

[103] S. Riemer-Sorensen, *Questioning a 3.5 keV dark matter emission line*, 1405.7943.